JOURNAL OF MODERN OPTICS, 1997, VOL. 44, NO. 3, 633–650

Focusing of axially symmetric flattened Gaussian beams

M. SANTARSIERO, D. AIELLO, R. BORGHI and S. VICALVI
Dipartimento di Fisica, Università 'La Sapienza' di Roma,
P.le A. Moro, 2; 00185 Rome, Italy

(*Received 13 August 1995*)

Abstract. We study the three-dimensional field distribution of a focused axially symmetric flattened Gaussian beam. In particular, exact closed-form expressions for the intensity along the optical axis and at the focal plane are provided, together with a comparison between our results and those pertinent to the case of a converging spherical wave diffracted by a hard-edge circular aperture. Some hints for future investigations are also given.

1. Introduction

Flattened Gaussian beams (FGBs) were introduced by Gori [1] as an efficient model to study the propagation features of beams showing, at a given waist plane, a flat-top profile. The interest in beams exhibiting such a behaviour is related to the fact that, in some applications, field distributions are required that are as flat as possible within a given area and almost vanish outside it. Furthermore, flattened profiles are also of interest in the study of the imaging properties of apodized pupils [2] and of optical resonators with variable-reflectivity mirrors [3, 4].

As a general rule of the propagation process, the flatness of a (transversally limited) coherent light profile must necessarily be lost upon propagation, and one can be interested in evaluating the field present at planes different from the waist plane. A limiting case consists of the problem of the diffraction of a plane wave by a circular hole, for which the flatness of the propagated profile is lost (at least within the framework of the paraxial approximation) for any, arbitrarily small distance from the screen. In this case the field profile at the waist plane is proportional to the function circ (r/a), a being the radius of the hole, and the propagation problem can be solved numerically, by means of the Lommel functions [5].

The most celebrated example of beams showing a flattened profile, the well known super-Gaussian beams [6], are characterized by a very simple expression at the waist plane but require specific numerical procedures in order to evaluate the propagated field [7, 8]. On the other hand, FGBs offer the advantage of being expressible as a finite sum of Laguerre–Gauss modes [9], and then the corresponding propagation problem can be solved exactly and does not require any numerical integration.

In [10] the free paraxial propagation of FGBs was studied, both theoretically and experimentally, and the M^2 factor for such beams was also evaluated. Some properties of FGBs in rectangular coordinates have been recently investigated in [11].

In the present paper we report some results pertinent to the case of a focused

FGB. In section 2 we recall the definition and the main paraxial propagation properties of FGBs, while in section 3 we consider the case of a focused FGB. In section 4 we give particular expressions for the focused field at the geometrical focal plane, along the optical axis and along the boundary of the geometrical shadow. Finally, in section 5 we show some results about the phase anomaly along geometrical rays passing through the focus.

2. Flattened Gaussian beams

In this section we briefly recall the definition and some properties of the FGBs. We introduce a reference frame with cylindrical coordinates (r, ψ, z), having the z axis and the $z = 0$ plane coincident with the propagation axis and the waist plane of the beam respectively. Since we shall study only axially symmetric field distributions, all the quantities used throughout the paper will be considered as depending on r and z alone, the angle ψ being immaterial. This choice corresponds to studying the field distribution across a meridional plane. Moreover, we suppose that a vectorial treatment is not required for the study of the involved fields, which will be described by scalar functions.

We define a FGB as a beam showing the following field distribution on the $z = 0$ plane [1, 10]:

$$U_N(r,0) = A_0 \exp\left(-\frac{(N+1)r^2}{w_0^2}\right) \sum_{n=0}^{N} \frac{1}{n!} \left(\frac{(N+1)r^2}{w_0^2}\right)^n, \tag{1}$$

where A_0 is a constant factor, w_0 is a positive parameter and N is an integer greater than or equal to zero. In figure 1, curves of $U_N(r,0)/A_0$ are shown as functions of r/w_0 for several values of N, together with the circ function. It can be seen that the

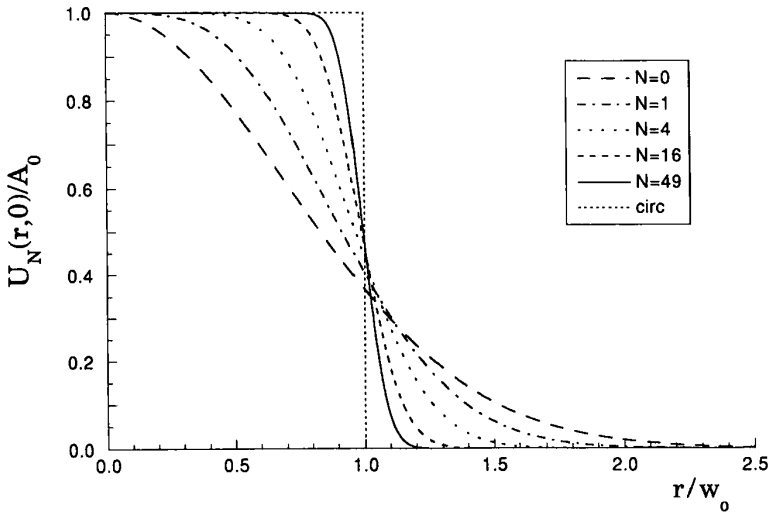

Figure 1. Flattened Gaussian profiles for different values of the parameter N, together with the circ function.

curve is Gaussian for $N = 0$, becomes more and more flattened on increasing N and tends to the function circ (r/w_0) when N goes to infinity. In conclusion, the shape of a FGB at its waist plane is characterized by two parameters, namely w_0 and N, denoting the width of the beam and the rapidity of the transition from the maximum value A_0 to zero respectively.

Although FGBs form a discrete family, whereas for example super-Gaussian beams furnish a continuous set, it is seen from equation (1) as well as from figure 1 that, except for the first few values of N, FGBs afford a rather dense set of functions and give, in practice, a tool for the study of flattened fields described by other analytical expressions, such as super-Gaussian beams [12].

As we said above, one of the most attractive properties of FGBs is that they can be expressed as the superposition of a finite number of Laguerre–Gauss beams [9]. In fact, the field (1) can be written in the form [1]

$$U_N(r) = A_0 \sum_{n=0}^{N} c_n^{(N)} L_n\left(\frac{2(N+1)r^2}{w_0^2}\right) \exp\left(-\frac{(N+1)r^2}{w_0^2}\right), \tag{2}$$

where L_n is the nth Laguerre polynomial [13] and the $c_n^{(N)}$ coefficients are defined as follows:

$$c_n^{(N)} = (-1)^n \sum_{m=n}^{N} \frac{1}{2^m} \binom{m}{n}. \tag{3}$$

Equation (2) states that the Nth-order FGB of width w_0 can be thought of as the sum, weighted by the coefficients $c_n^{(N)}$, of the first N Laguerre–Gauss beams, all having the same waist size

$$w_N(0) = \frac{w_0}{(N+1)^{1/2}}. \tag{4}$$

Some of the properties of the $c_n^{(N)}$ coefficients have been reported in [10], where a useful recurrence relation was also derived.

Finally, we recall the expression of a FGB propagated through a paraxial symmetric optical system, characterized by an $ABCD$ matrix [9]. Under the non-restrictive hypothesis that the input plane coincides with the waist plane of the beam, the output field turns out to be [10]

$$U_N(r,1) = A_0 \frac{w_N(0)}{w_N(1)} \exp\left[\mathrm{i}kl + \left(\frac{\mathrm{i}k}{2R_N(1)} - \frac{1}{w_N^2(1)}\right)r^2\right] \times \sum_{n=0}^{N} c_n^{(N)} L_n\left(\frac{2r^2}{w_N^2(1)}\right) \exp\left[-\mathrm{i}(2n+1)\Phi_N(1)\right], \tag{5}$$

where the indexes 0 and 1 denote the input and the output planes respectively of the system, k is the wavenumber, l is the optical length measured along the optical

axis, and the following relations have been used:

$$w_N(1) = |A| w_N(0)(1 + G^2)^{1/2}, \tag{6a}$$

$$R_N(1) = AB \frac{1 + G^{-2}}{1 + BC(1 + G^{-2})}, \tag{6b}$$

$$\Phi_N(1) = \tan^{-1} G, \tag{6c}$$

where

$$G = \frac{B}{A} \frac{2}{k w_N^2(0)}, \tag{7}$$

and A, B and C are the elements of the pertaining $ABCD$ matrix.

In the next section we shall specialize these results to the case of an optical system giving rise to a focused FGB.

3. Focusing of flattened Gaussian beams

In the paraxial regime, a converging FGB is obtained by superimposing a quadratic phase modulation, with a negative curvature radius, say $-f$, to the field given by equation (1). The resulting field in the plane $z = 0$ is

$$U_N(r, 0) = A_0 \exp\left[- \left(\mathrm{i} \frac{k}{2f} + \frac{(N+1)}{w_0^2} \right) r^2 \right] \sum_{n=0}^{N} \frac{1}{n!} \left(\frac{(N+1) r^2}{w_0^2} \right)^n. \tag{8}$$

To obtain the expression of the field propagated at a distance z, starting from the distribution (8), we have simply to apply the results of the previous section to an optical system consisting in one thin converging lens with focal length f placed in the input plane. Moreover, the plane at a distance z beyond the lens is the output plane. The $ABCD$ matrix for such system will be given by the product of the matrices corresponding to the thin lens and the free propagation, that is

$$\begin{bmatrix} A & B \\ C & D \end{bmatrix} = \begin{bmatrix} 1 & z \\ 0 & 1 \end{bmatrix} \begin{bmatrix} 1 & 0 \\ -\frac{1}{f} & 1 \end{bmatrix} = \begin{bmatrix} 1 - \frac{z}{f} & z \\ -\frac{1}{f} & 1 \end{bmatrix}, \tag{9}$$

and the length l in equation (5) must be taken as z.

Furthermore, following the classical theory of Lommel [5], we introduce the dimensionless coordinates

$$v = \frac{F}{w_0} r, \qquad u = \frac{F}{f} (z - f), \tag{10}$$

where the parameter

$$F = \frac{k w_0^2}{f} \tag{11}$$

is proportional to the Fresnel number N_F [9] by a factor 2π.

Using these new variables, the propagated field (5) can be written as

$$U'_N(v,u) = \frac{A_0 F}{\alpha_N(u)} \exp\left\{ i\left[kf + \left(\frac{f}{w_0}\right)^2 u + \frac{v^2}{2\beta_N(u)} \right] \right\} \times \exp\left(-\frac{(N+1)}{\alpha_N^2(u)} v^2 \right) \sum_{n=0}^{N} c_n^{(N)} L_n\left(\frac{2(N+1)}{\alpha_N^2(u)} v^2 \right) \exp\left[-i(2n+1)\gamma_N(u)\right], \tag{12}$$

where

$$\alpha_N(u) = \left(1 + \frac{u}{F}\right)\left[\left(\frac{u}{1+u/F}\right)^2 + 4(N+1)^2\right]^{1/2}, \tag{13a}$$

$$\beta_N(u) = F\left(1 + \frac{u}{f}\right)\frac{4(N+1)^2 + [u/(1+u/F)]^2}{4(N+1)^2 + Fu/(1+u/F)}, \tag{13b}$$

$$\gamma_N(u) = \tan^{-1}\left[-\frac{2(N+1)}{u}\left(1 + \frac{u}{F}\right)\right]. \tag{13c}$$

These quantities are obtained by introducing the values of A, B and C, given by equation (9), into equations (6 *a*)–(6 *c*) and (7), and by using the definitions (10) and (11). In equation (12) and in the following we add a prime to distinguish the functions of v and u from those pertinent to the same quantities but considered as functions of r and z.

Let us introduce, for convenience, the (complex) function

$$H_N(v,u) = \frac{1}{\alpha_N(u)} \exp\left(-\frac{(N+1)}{\alpha_N^2(u)} v^2 \right) \times \sum_{n=0}^{N} c_n^{(N)} L_n\left(\frac{2(N+1)}{\alpha_N^2(u)} v^2 \right) \exp\left[-i(2n+1)\gamma_N(u)\right], \tag{14}$$

and denote its phase by $\chi_N(v,u)$. Then, the focused field can be written as

$$U'_N(v,u) = A_0 F H_N(v,u) \exp\left\{ i\left[kf + \left(\frac{f}{w_0}\right)^2 u + \frac{v^2}{2\beta_N(u)} \right] \right\} \tag{15}$$

and, in particular, its intensity and phase will be given by

$$I'_N(v,u) = A_0^2 F^2 |H_N(v,u)|^2 \tag{16}$$

and

$$\phi'_N(v,u) = kf + \left(\frac{f}{w_0}\right)^2 u + \frac{v^2}{2\beta_N(u)} + \chi_N(v,u). \tag{17}$$

The field obtained following these lines represents the exact solution of the propagation problem, for any choice of the values of N and F. However, in order to simplify equations (13 *a*)–(13 *c*), it is convenient to consider their limiting

behaviour for large values of F, that is to require that

$$|u| \ll F, \tag{18}$$

with u and v being kept fixed. From definitions (10) and (11), it follows that this requirement is equivalent to keeping the observation point as well as the wavelength and the angular semiaperture w_0/f fixed and letting $f \to \infty$ [14]. This is exactly the condition under which the classical formulation of Lommel is derived [15]. We shall see in the following how, starting from the results obtained in this limit, one can easily derive the exact results, valid for any choice of F.

Hence, by adopting the approximation (18), equations (13 *a*)–(13 *c*) for the propagation parameters become

$$\alpha_N(u) \approx [4(N+1)^2 + u^2]^{1/2}, \tag{19a}$$

$$\beta_N(u) \approx F\frac{4(N+1)^2 + u^2}{4(N+1)^2 + Fu}, \tag{19b}$$

$$\gamma_N(u) \approx \frac{\pi}{2} + \tan^{-1}\left(\frac{u}{2(N+1)}\right). \tag{19c}$$

On inserting equations (19 *a*) and (19 *c*) into equation (14) and from the latter into equation (16) we see that in the present limit, once N has been chosen, the intensity profile is completely specified (apart from the overall factor F^2). On the other hand, to evaluate the phase profile, one has to fix the numerical aperture of the system ($f_{\#} = f/2w_0$), as well as the Fresnel number ($N_F = F/2\pi$), on which ϕ'_N still depends (see equations (17) and (19 *b*)).

In figures 2 (*a*), (*b*), (*c*) and (*d*) contour plots of the intensity (isophotes) on the (u, v) plane are shown for $N = 1$, $N = 4$, $N = 16$ and $N = 100$ respectively. In that figure, labels refer to ten times the common logarithm of the intensity. The latter is normalized with respect to its maximum value. As stated above, these curves are independent of the Fresnel number and the numerical aperture, and they show symmetry with respect to both axes. From the analysis of these curves it can be noticed that, on increasing N, the intensity distribution at the focal plane widens, as was expected, and, conversely, the depth of focus increases. This means that, in some applications, an optimum value of the order of the FGB could be chosen for a trade-off between focused power and depth of focus. Furthermore, the intensity pattern at the focal plane has dark rings. In the next section we shall see that the number of these dark rings equals the order of the FGB.

The curves in figures 2 (*a*)–(*d*) should be compared with the celebrated curves appearing in the paper by Linfoot and Wolf [16] (see also [5]) obtained by means of the Lommel functions, for the case of a converging spherical wave diffracted by a circular aperture. For convenience, the Linfoot–Wolf curves are redrawn in figure 2 (*e*). It is seen that, on increasing N, the curves obtained by equation (16) become more and more similar to those of figure 2 (*e*).

In figure 3, grey-level plots are presented for the phase of the field, in the proximity of the focal plane, for the same values of the order N (with $f_{\#} = 3{\cdot}5$ and $F = 10^3$). We can note that dislocations of the phase appear to correspond to the zeros of the intensity distribution.

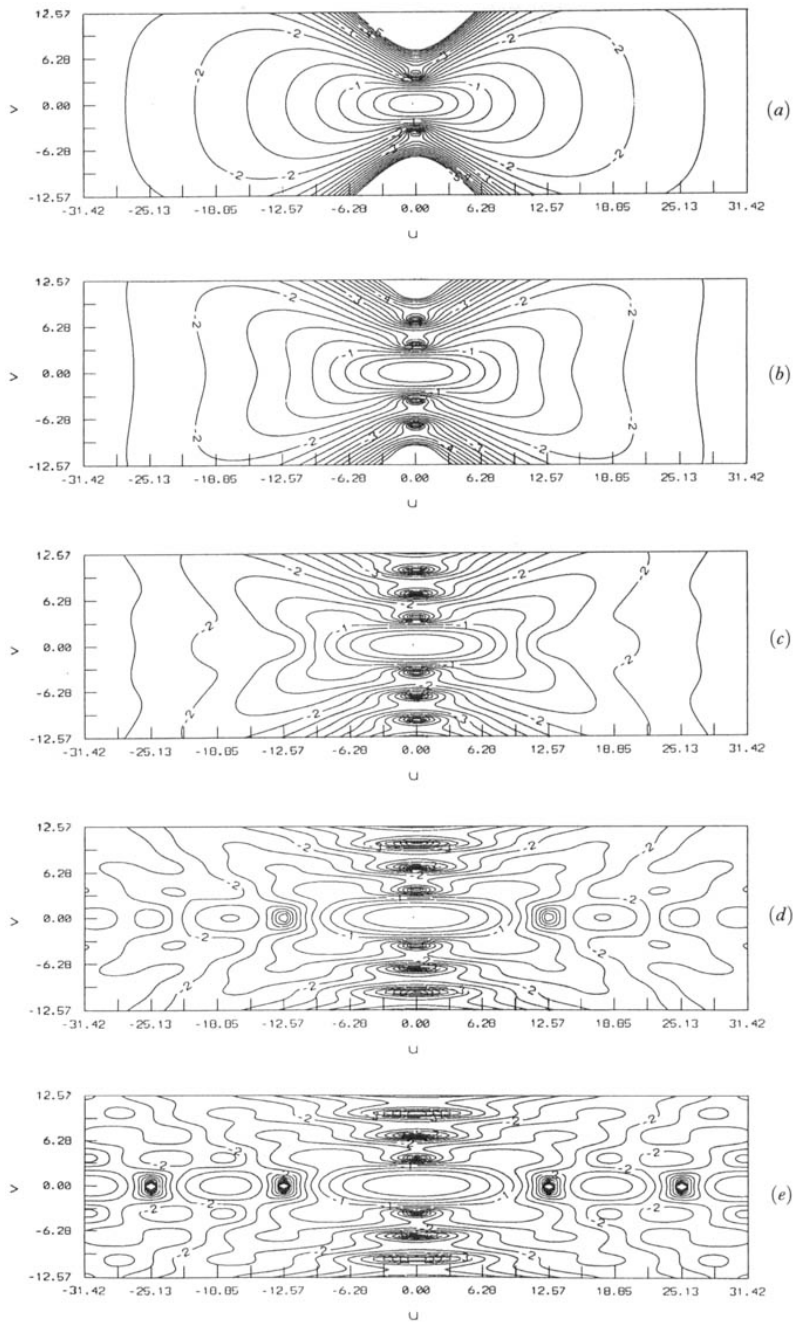

Figure 2. Isophotes in the (u,v) plane for focused FGBs near focus for (*a*) $N = 1$, (*b*) $N = 4$, (*c*) $N = 16$ and (*d*) $N = 100$. (*e*) The case of a converging spherical wave diffracted by a circular hole.

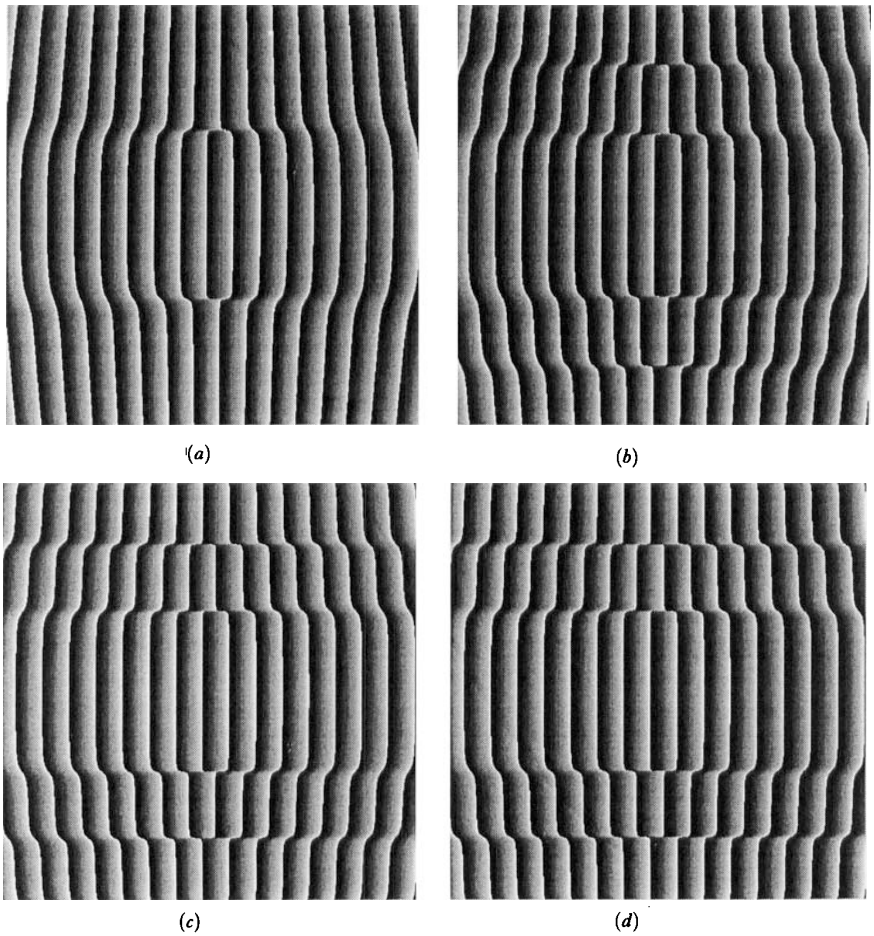

Figure 3. Grey-level plots of the phase for focused FGBs in the (u, v) plane near focus for (*a*) $N = 1$, (*b*) $N = 4$, (*c*) $N = 16$ and (*d*) $N = 100$.

Before concluding this section, we briefly point out how to extend the results obtained in the limit of large Fresnel numbers to the most general case [14]. The exact expression of the focused field, in fact, coincides with the approximate expression, provided that the variables v and u are replaced by the new variables

$$v_F = \frac{v}{1 + u/F}, \qquad u_F = \frac{u}{1 + u/F}, \tag{20}$$

and that the values of amplitude and phase are corrected by means of the factor $1 - u_F/F$.

The most evident effect of non-negligible values of u/F on the field profiles is due to the fact that the relationship between the variables (v_F, u_F) and the physical coordinates (r, z) is nonlinear. In fact, when the Fresnel number is not large

enough, this nonlinearity causes the diagrams of the isophotes, when considered as functions of the physical coordinates, to be distorted with respect to those shown in figure 3. In particular, the point where the maximum of the intensity is observed, which in figure 2 coincides with the geometrical focus, appears to be shifted towards the lens, and the symmetry with respect to the $z = f$ axis is lost. This effect is related to the well known focal shift that occurs in the focusing of optical fields with low Fresnel numbers [17–20]. An accurate description of the deformations induced by the relations (20) can be found in [14].

4. Field distribution in some particular cases

Starting from equation (15) and using the definitions (14) and (19*a*)–(19*c*) it is possible to evaluate the field distribution for some particular cases. In this section we shall deduce the expressions of the focused field in the focal plane, on the optical axis and along the boundary of the geometrical shadow.

4.1. *Field in the geometrical focal plane*

In this case we have $u = 0$, whence it can be easily seen, from equations (19*a*)–(19*c*), that

$$\alpha_N(0) = 2(N+1), \tag{21a}$$

$$\beta_N(0) = F, \tag{21b}$$

$$\gamma_N(0) = \frac{\pi}{2}, \tag{21c}$$

and, from equations (14) and (17), that

$$H_N(v,0) = \frac{-\mathrm{i}}{2(N+1)} \exp\left(-\frac{v^2}{4(N+1)}\right) \sum_{n=0}^{N} c_n^{(N)} (-1)^n L_n\left(\frac{v^2}{2(N+1)}\right) \tag{22}$$

and

$$\phi'_N(v,0) = kf - \frac{\pi}{2} + \frac{v^2}{2F}. \tag{23}$$

The sum in equation (22) can be evaluated starting from the definition (3) of the $c_n^{(N)}$ coefficients, and by exploiting some properties of the Laguerre polynomials [13], and the resulting field (15) is

$$U'_N(v,0) = \frac{-\mathrm{i}A_0 F}{2(N+1)} \exp\left[\mathrm{i}\left(kf + \frac{v^2}{2F}\right)\right] L_N^{(1)}\left(\frac{v^2}{4(N+1)}\right) \exp\left(-\frac{v^2}{4(N+1)}\right), \tag{24}$$

where the Laguerre polynomial with indexes N and 1 has been introduced [13]. As is well known [5], this expression is related to that giving the field produced in the far zone by a non-focused FGB and in fact coincides, apart from phase factors, with the expression given in [10] for the far-field limit. Therefore, as for the case treated in [10], it is possible to show that the field (24) tends, when N goes to

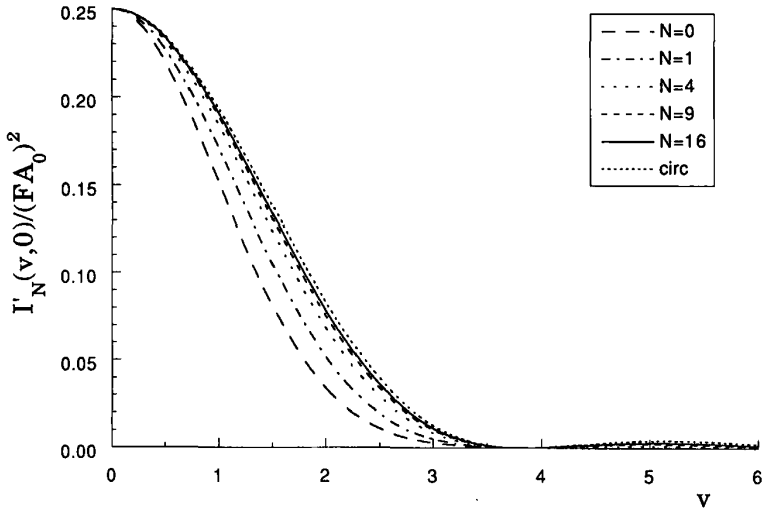

Figure 4. Intensity profile of focused FGBs on the focal plane, for different values of N, together with the case corresponding to the circ function.

infinity, to the diffraction pattern for a circular hole, that is

$$U'_\infty(v,0) = -iA_0F \exp\left[i\left(kf + \frac{v^2}{2F}\right)\right]\frac{J_1(v)}{v}, \tag{25}$$

where J_1 is the Bessel function of the first type of order 1.

It is worth noting that, since in the focal plane $u_F = u = 0$ and $v_F = v$, equations (24) and (25) keep their validity for any choice of the Fresnel number, because condition (18) is always fulfilled.

In figure 4, curves of the intensity of the function (24) are shown, for several values of N, together with that pertinent to the function (25) (dotted curve). It can be seen that in the central zone the intensity of the field is well approximated by its limiting curve even for small values of N, while the difference becomes more and more evident as the radial coordinate increases. Finally, the presence of the Nth-order Laguerre polynomial in equation (24) ensures that the diffraction pattern shows exactly N dark rings in the focal plane.

4.2. *Field along the optical axis*

In this section we show some results pertaining to the case in which $v = 0$, corresponding to the points lying on the optical axis. Letting $v = 0$ in equation (14), we get

$$H_N(0,u) = \frac{1}{\alpha_N(u)}\sum_{n=0}^{N} c_n^{(N)} \exp\left[-i(2n+1)\gamma_N(u)\right], \tag{26}$$

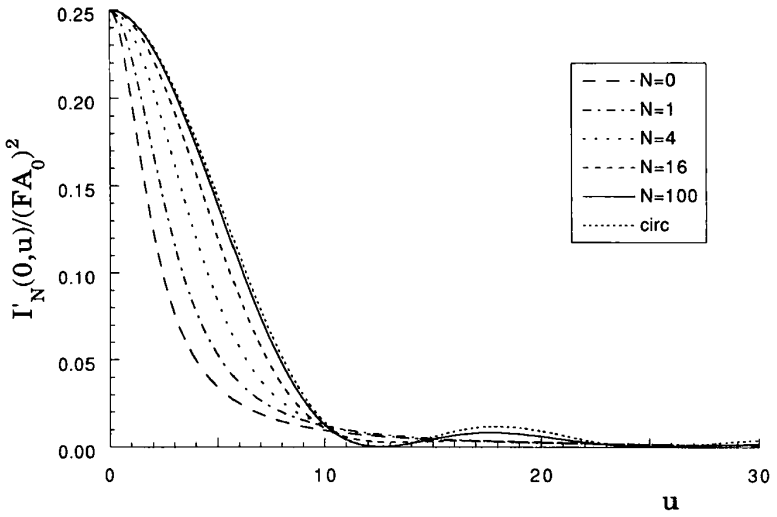

Figure 5. On-axis intensity of focused FGBs, for different values of N, together with the case corresponding to the circ function.

which, from equation (3), becomes [10]

$$H_N(0,u) = \frac{1 - \sin^{N+1}[\gamma_N(u)] \exp\{i(N+1)[\pi/2 - \gamma_N(u)]\}}{\alpha_N(u) \cos[\gamma_N(u)]}. \tag{27}$$

Moreover, by using equation (19*c*), after some calculations we obtain

$$U'_N(0,u) = A_0 F \exp\left\{i\left[kf + \left(\frac{f}{w_0}\right)^2 u\right]\right\} \frac{[1 + iu/2(N+1)]^{-(N+1)} - 1}{u}. \tag{28}$$

In this case, too, it is possible to perform the limit for $N \to \infty$, yielding

$$U'_\infty(0,u) = \frac{-iA_0 F}{2} \exp\left\{i\left[kf + \left(\frac{f}{w_0}\right)^2 u - \frac{u}{4}\right]\right\} \frac{\sin(u/4)}{u/4}, \tag{29}$$

in agreement with the results given by the Lommel theory [5]. It should be noted that, while in this limiting case the on-axis intensity shows zeros (evenly spaced, except for $u = 0$, with period $\Delta u = 4\pi$), this is not the case for any finite values of N, because the modulus of the function (28) never vanishes. Plots of the intensity of the function (28) are shown in figure 5 for several values of N, together with that of the limiting function (29) (dotted curve).

4.3. *Field along the boundary of the geometrical shadow*

In the study of the diffraction of a spherical wave by a circular aperture, a quantity that can be easily evaluated is the field along the boundary of the geometrical shadow [5]. In this section we show the analogous quantity, pertinent to the case of a focused FGB. More precisely, since in this case a geometrical

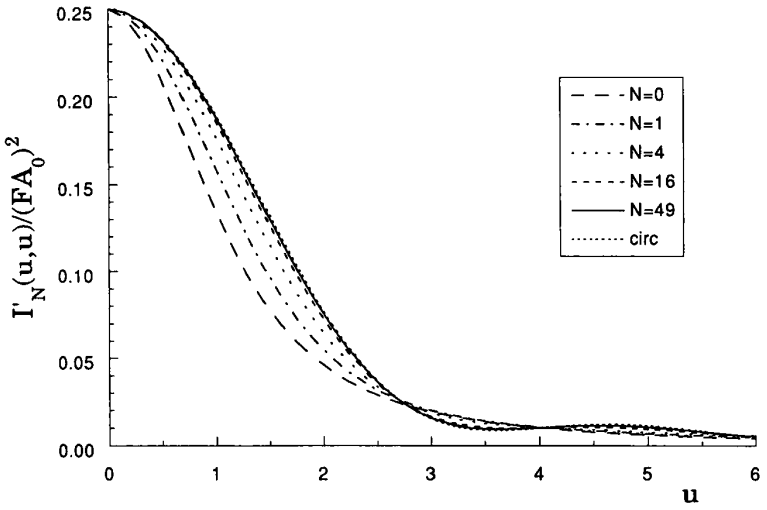

Figure 6. Intensity profile of focused FGBs along the boundary of the geometrical shadow, for different values of N, together with the case corresponding to the circ function.

shadow cannot be defined in a rigorous way (except in the limit $N \to \infty$), we shall study the field along lines passing through the focus and the coordinate $r = w_0$ of the $z = 0$ plane. These lines are represented in the (r, z) plane by the equations

$$r = \pm \frac{w_0}{f}(f - z), \tag{30}$$

or by use of the pertinent dimensionless variables

$$v = \pm u. \tag{31}$$

In figure 6 plots of the intensity of the focused field evaluated along the line $v = u$ are shown, for different values of N. It is evident that, since the field is axially symmetric, it is immaterial to choose the + or the − sign in equation (31). In the same figure, the limiting curve, evaluated through the relation [5]

$$I'_\infty(u,u) = \left(\frac{A_0 F}{2}\right)^2 \frac{1 - 2J_0(u)\cos u + J_0^2(u)}{u^2}, \tag{32}$$

is shown by a dotted curve.

5. The phase anomaly

In this section we study how the phase of the field changes as the observation point moves along a ray passing through the focus. Instead of the phase $\phi_N(r, z)$ of the focused field, however, it is convenient to visualize the so-called phase anomaly $\delta(r, z)$. The latter is defined as the difference between ϕ_N and the phase of a

spherical wave converging to the focus. In formulae we have

$$\delta(r,z) = \phi_N(r,z) - \tilde{\phi}(r,z), \tag{33}$$

where

$$\tilde{\phi}(r,z) = \begin{cases} -k\rho, \\ +k\rho, \end{cases} \quad \text{if} \quad \begin{cases} z < f, \\ z > f, \end{cases} \tag{34}$$

and

$$\rho = [r^2 + (z-f)^2]^{1/2}. \tag{35}$$

By recalling the definitions (10) of the dimensionless variables v and u and the expression for the phase of the focused field (equation (17)), we obtain

$$\delta'_N(v,u) = \left(\frac{f}{w_0}\right)^2 u - \operatorname{sgn}(u)\frac{f}{w_0}\left[\left(\frac{f}{w_0}\right)^2 u^2 + v^2\right]^{1/2} + \frac{v^2}{2\beta_N(u)} + \chi_N(v,u), \tag{36}$$

where the constant term kf, present in equation (17), has been omitted and the signum function sgn (u) has been used.

In figures 7, 8 and 9 the phase anomaly of focused FGBs with $f_{\#} = 3{\cdot}5$ and $F = 10^3$ is shown for $N = 4$, 16 and 100 respectively. The inclination angles ϑ are chosen as 8·13° (corresponding to the boundary of the geometrical shadow), 4°, 2° and 0°. In figure 10 the same quantities are calculated for the case of a spherical wave diffracted by a circular hole, by using the Lommel functions.

In each case it can be noted that the phase anomaly undergoes a continuous change of $-\pi$ on passing through the focus. Such change is more rapid for high values of the angle ϑ and is observed for every value of N. This effect was predicted long ago by Gouy [21] and has been the subject of many investigations, even recently [16, 22–25].

Finally, we note that, in the case of a ray along the optical axis (figure 10), the phase anomaly tends, for high values of N, to a linear function, with discontinuities at values of u multiples of 4π (except for $u = 0$), and this behaviour is independent of both the numerical aperture of the beam and the Fresnel number. This is because in this case the anomaly is given, apart from constant terms, by $u/4 \pm \pi/2$ (see equations (29) and (36)), where the sign is determined by the sign of the function $[\sin(u/4)]/(u/4)$.

6. Conclusions

In this paper the field produced by a converging FGB has been evaluated, and plots of both the intensity and the phase distributions have been presented. We showed that the quantities evaluated for a converging FGB, such as the field across the focal plane and along geometrical rays passing through the focus, tend, on increasing the order of the beam, to those pertinent to a converging spherical wave diffracted by a circular hole.

In particular, owing to the analytical structure of FGBs, the propagated field can be exactly evaluated starting from the propagation features of Laguerre–Gauss modes, and very simple closed-form expressions can be given for the field along the optical axis and across the focal plane.

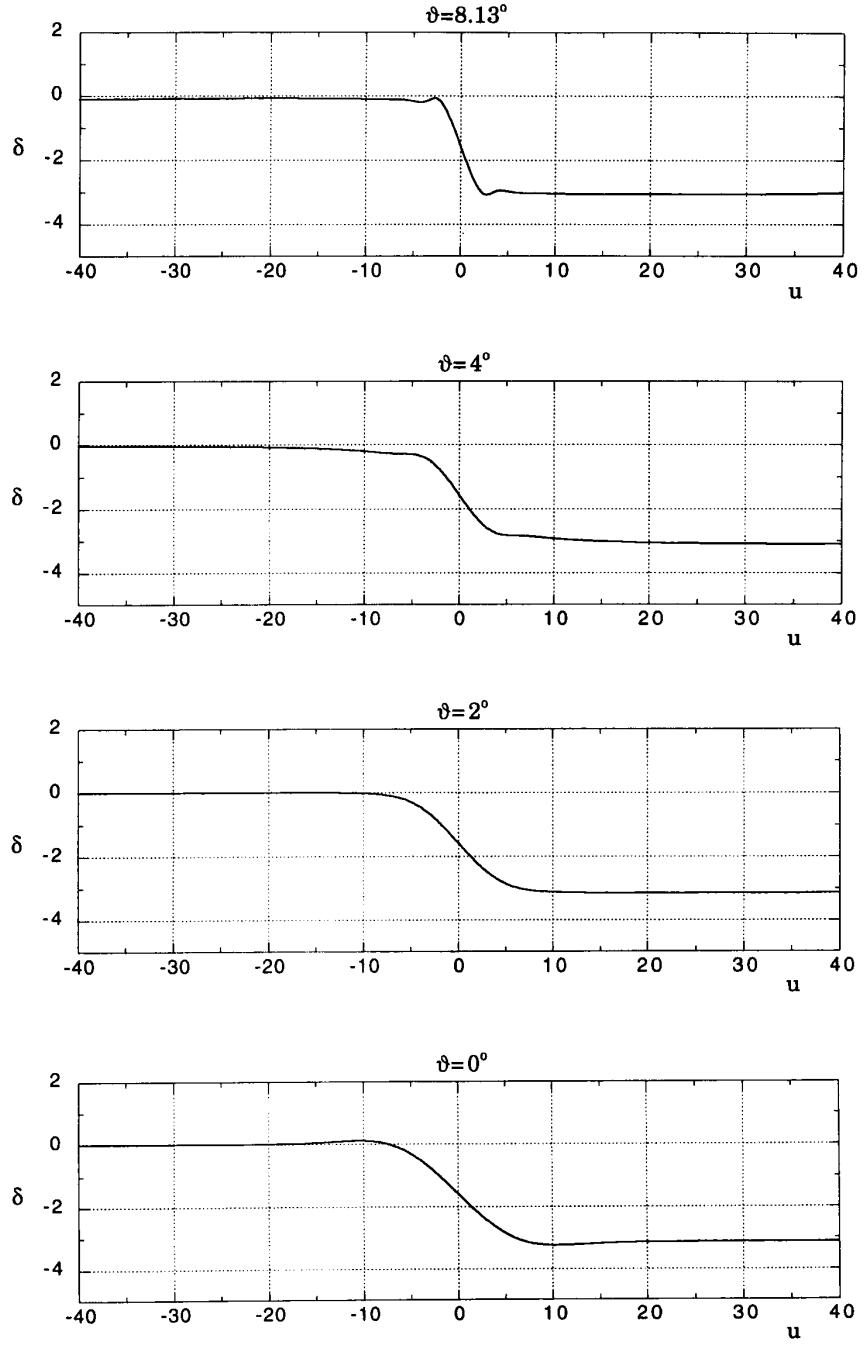

Figure 7. Phase anomaly for the focused FGB with $f_{\#} = 3{\cdot}5$ and $F = 10^3$, along different geometrical rays passing through the focus (the angle ϑ denotes inclination of the ray to the axis). The order of the beam is $N = 4$.

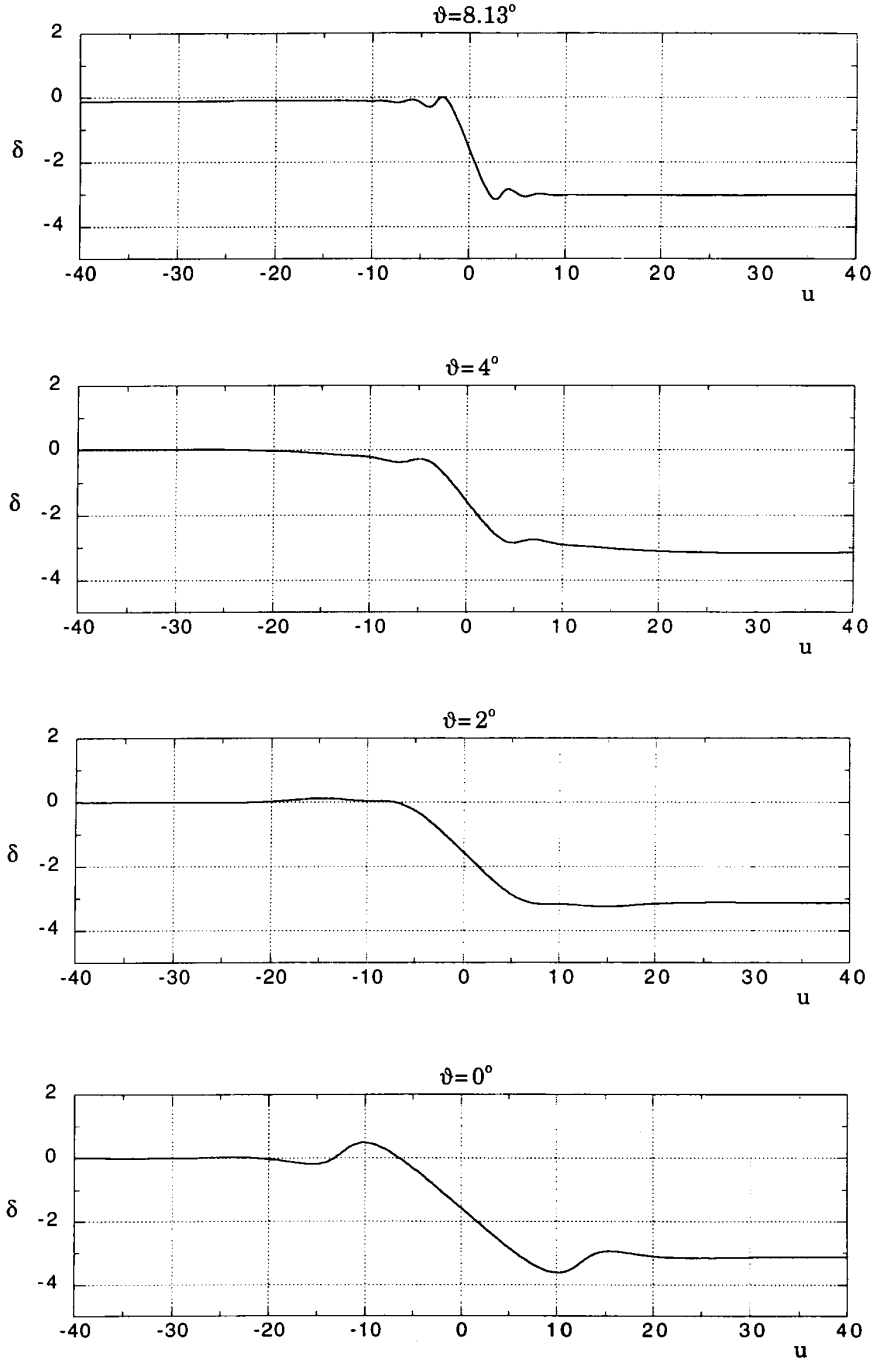

Figure 8. The same as in figure 7 but for a FGB of order $N = 16$.

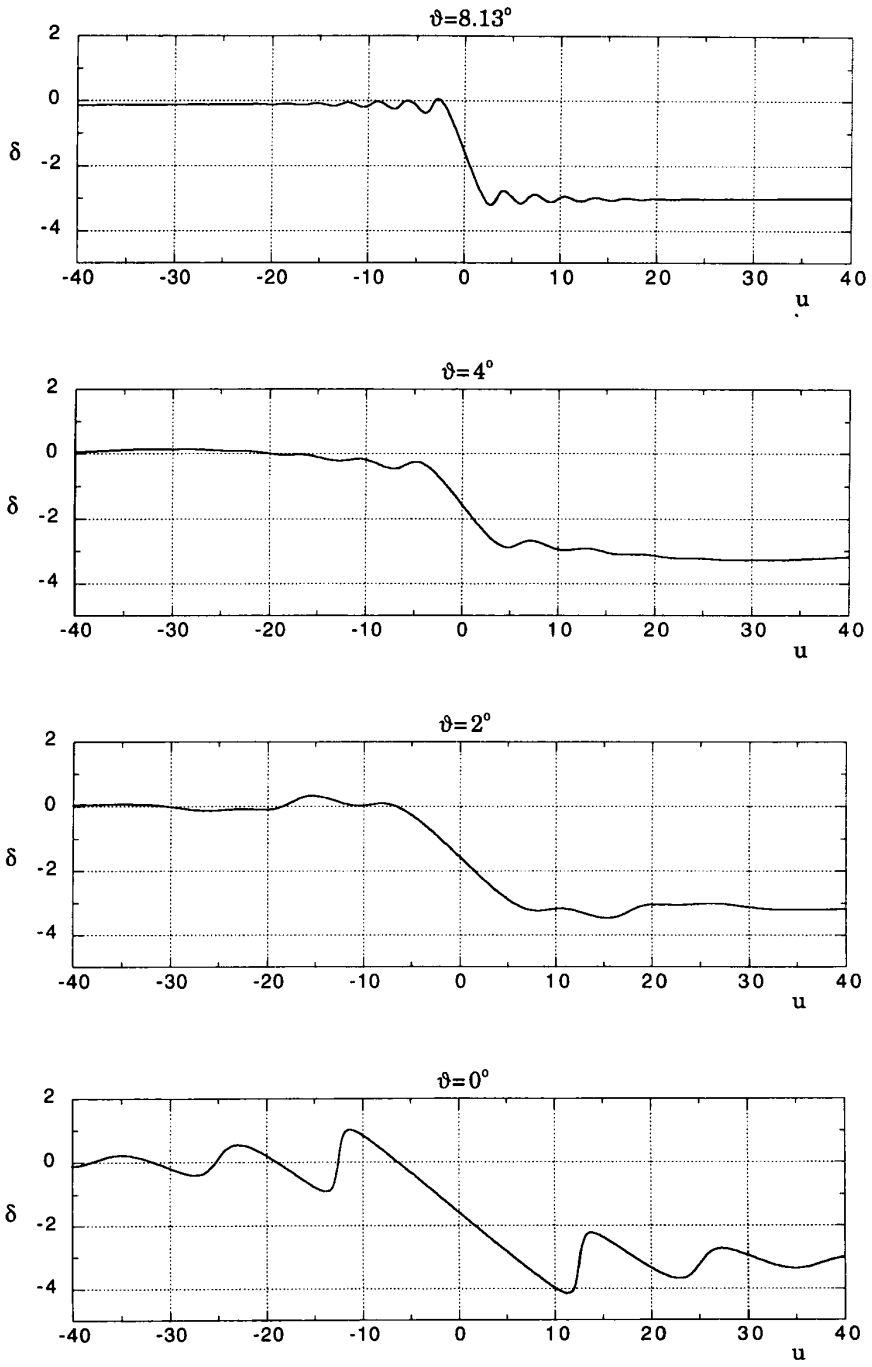

Figure 9. The same as in figure 7 but for a FGB of order $N = 100$.

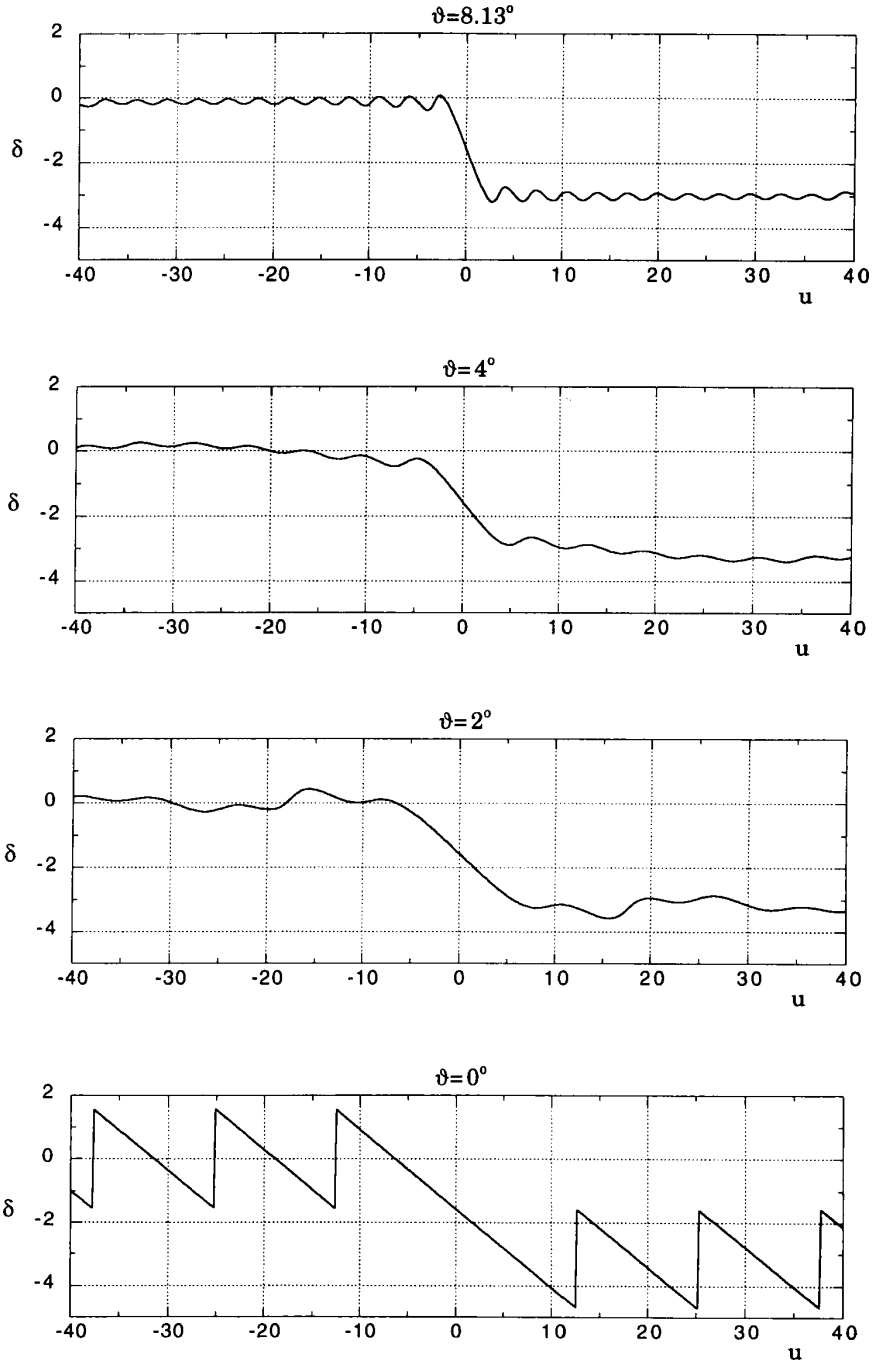

Figure 10. The same as in figure 7 but for a converging spherical wave diffracted by a circular aperture.

Our results confirm the fact that the family of FGBs is an attractive example of flat-top beams and could be useful for several applications, such as the study of optical resonators with variable-reflectivity mirrors or the design of optical systems with an apodized pupil.

Finally, this model could be profitably used to calculate other useful quantities, such as the total power falling onto a circle centred on the optical axis at a plane parallel to the focal plane, or the focal shift of focused flattened beams.

Acknowledgments

We wish to thank Franco Gori for useful and stimulating discussions. This work was supported by Istituto Nazionale per la Fisica della Materia and Ministero dell'Università e della Ricerca Scientifica e Tecnologica.

References

[1] Gori, F., 1994, *Optics Commun.*, **107,** 335.
[2] Sheppard, C. J. R., 1996, *J. mod. Optics*, **43,** 525.
[3] Perrone, M R., Piegari, A., and Scaglione, S., 1993, *IEEE Jl quant. Electron.*, **29,** 1423.
[4] Bélanger, P. A., Lachance, R. L., and Paré, C., 1991, *Optics Lett.*, **17,** 739.
[5] Born, M., and Wolf, E., 1993, *Principles of Optics*, sixth edition, reprinted (Oxford: Pergamon), chapter 8.
[6] De Silvestri, S., Laporta, P., Magni, V., and Svelto, O., 1988, *IEEE Jl quant. Electron.*, **24,** 1172.
[7] Parent, A., Morin, M., and Lavigne, P., 1992, *Opt. quant. Electron.*, **24,** 1071.
[8] Lü, B., Zhang, B., and Wang, X., 1996, *Optics Commun.*, **126,** 1.
[9] Siegman, A., 1986, *Lasers* (Mill Valley, California: University Science).
[10] Bagini, V., Borghi, R., Gori, F., Pacileo, A. M., Santarsiero, M., Ambrosini, D., and Schirripa Spagnolo, G., 1996, *J. opt. Soc. Am.* A, **13,** 1385.
[11] Amarande, S.-A., 1996, *Optics Commun.*, **129,** 311.
[12] Palma, C., and Bagini, V., 1994, *Optics Commun.*, **111,** 6.
[13] Abramowitz, M., and Stegun, I. (editors), 1972, *Handbook of Mathematical Functions* (New York: Dover Publications), chapter 22.
[14] Li, Y., and Wolf, E., 1984, *J. opt. Soc. Am.* A, **1,** 801.
[15] Wolf, E., and Li, Y., 1981, *Optics Commun.*, **39,** 205.
[16] Linfoot, E. H., and Wolf, E., 1956, *Proc. phys. Soc.* B, **69,** 823.
[17] Li, Y., and Wolf, E., 1981, *Optics Commun.*, **39,** 211.
[18] Li, Y., and Wolf, E., 1982, *Optics Commun.*, **42,** 151.
[19] Poon, T.-C., 1988, *Optics Commun.*, **65,** 401.
[20] Lü, B., and Huang, W., 1994, *Optics Commun.*, **109,** 43.
[21] Gouy, L. G., 1890, *C. r. hebd. Séanc. Acad. Sci., Paris*, **110,** 1251.
[22] Rubinowicz, A., 1938, *Phys. Rev.*, **54,** 931.
[23] Farnell, G. W., 1958, *Can. J. Phys.*, **36,** 935.
[24] Subbarao, D., 1995, *Optics Lett.*, **20,** 2162.
[25] Hariharan, P., and Robinson, P. A., 1996, *J. mod. Optics*, **43,** 219.